Earth and Planetary Science Letters 361 (2013) 152–161

Contents lists available at SciVerse ScienceDirect

Earth and Planetary Science Letters

journal homepage: www.elsevier.com/locate/epsl

Coupled W–Os–Pt isotope systematics in IVB iron meteorites: In situ neutron dosimetry for W isotope chronology

N. Wittig [a,*], M. Humayun [a], A.D. Brandon [b], S. Huang [a,c], I. Leya [d]

[a] Department of Earth, Ocean and Atmospheric Science & National High Magnetic Field Laboratory, 1800 E. Paul Dirac Drive, Florida State University, Tallahassee, FL 32310, USA
[b] Department of Earth and Atmospheric Sciences, University of Houston, 312 Science & Research 1, Houston, TX 77204, USA
[c] Department of Earth and Planetary Sciences, Harvard University, 20 Oxford St., Cambridge, MA 02138, USA
[d] Physical Institute, Space Science and Planetology, University of Bern, Sidlerstrasse 5, 3012 Bern, Switzerland

ARTICLE INFO

Article history:
Received 18 June 2012
Received in revised form
8 October 2012
Accepted 11 October 2012
Editor: T. Elliott
Available online 27 November 2012

Keywords:
IVB iron meteorites
geochronology
galactic cosmic rays
W, Pt and Os isotopes
nucleosynthetic anomalies

ABSTRACT

Tungsten isotope compositions of magmatic iron meteorites yield ages of differentiation that are within ± 2 Ma of the formation of CAIs, with the exception of IVB irons that plot to systematically less radiogenic compositions yielding erroneously old ages. Secondary neutron capture due to galactic cosmic ray (GCR) irradiation is known to lower the ε^{182}W of iron meteorites, adequate correction of which requires a measure of neutron dosage which has not been available, thus far. The W, Os and Pt isotope systematics of 12 of the 13 known IVB iron meteorites were determined by MC-ICP-MS (W, Os, Pt) and TIMS (Os). On the same dissolutions that yield precise ε^{182}W, stable Os and Pt isotopes were determined as in situ neutron dosimeters for empirical correction of the ubiquitous cosmic-ray induced burn-out of ^{182}W in iron meteorites. The W isotope data reveal a main cluster with ε^{182}W of ~ -3.6, but a much larger range than observed in previous studies including irons (Weaver Mountains and Warburton Range) that show essentially no cosmogenic effect on their ε^{182}W. The IVB data exhibits resolvable negative anomalies in ε^{189}Os (-0.6ε) and complementary ε^{190}Os anomalies ($+0.4\varepsilon$) in Tlacotepec due to neutron capture on ^{189}Os which has approximately the same neutron capture cross section as ^{182}W, and captures neutrons to produce ^{190}Os. The least irradiated IVB iron, Warburton Range, has ε^{189}Os and ε^{190}Os identical to terrestrial values. Similarly, Pt isotopes, which are presented as ε^{192}Pt, ε^{194}Pt and ε^{196}Pt range from $+4.4\varepsilon$ to $+53\varepsilon$, $+1.54\varepsilon$ to -0.32ε and $+0.73\varepsilon$ to -0.20ε, respectively, also identify Tlacotepec and Dumont as the most GCR-damaged samples. In W–Os and W–Pt isotope space, the correlated isotope data back-project toward a 0-epsilon value of ε^{192}Pt, ε^{189}Os and ε^{190}Os from which a pre-GCR irradiation ε^{182}W of -3.42 ± 0.09 (2σ) is derived. This pre-GCR irradiation ε^{182}W is within uncertainty of the currently accepted CAI initial ε^{182}W. The Pt and Os isotope correlations in the IVB irons are in good agreement with a nuclear model for spherical irons undergoing GCR spallation, although this model over-predicts the change of ε^{182}W by $\sim 2\times$, indicating a need for better W neutron capture cross section determinations. A nucleosynthetic effect in ε^{184}W in these irons of -0.14 ± 0.08 is confirmed, consistent with the presence of Mo and Ru isotope anomalies in IVB irons. The lack of a non-GCR Os isotope anomaly in these irons requires more complex explanations for the production of W, Ru and Mo anomalies than nebular heterogeneity in the distribution of s-process to r-process nuclides.

1. Introduction

The ^{182}Hf–^{182}W chronometer ($t_{1/2}$=8.9 Ma) is important for dating metal-silicate fractionation events in the first 60 Ma of solar system history (Jacobsen, 2005; Kleine et al., 2009). The initial W isotope composition and the $(^{182}Hf/^{180}Hf)_0$ ratio are essential for calibration of this chronometer. In the first attempts to apply the Hf–W isotope chronometer, the least radiogenic W in solar system material was obtained from precise W isotopic analyses of iron meteorites yielding initial ε^{182}W~ -4 (Harper and Jacobsen, 1996; Lee and Halliday, 1996). Precise Hf–W isochrons on Allende CAIs have yielded refined values of ε^{182}W$=-3.28 \pm 0.12$ (Burkhardt et al., 2008), although this value may be compromised by metamorphism of Allende (Humayun et al., 2007). Recently, the CAI initial ε^{182}W has been revised (-3.51 ± 0.10 2σ) to account for nucleosynthetic anomalies in the

* Corresponding author. Present address: Department of Earth Sciences and Isotope Geochemistry and Geochronology Research Centre, 2125 Herzberg Building, Carleton University, 1125 Colonel By Drive, Ottawa, Ontario, Canada K1S 5B6.
E-mail addresses: wittig@magnet.fsu.edu (N. Wittig), humayun@magnet.fsu.edu (M. Humayun).

0012-821X/$ - see front matter © 2012 Elsevier B.V. All rights reserved.
http://dx.doi.org/10.1016/j.epsl.2012.10.013

original data (Burkhardt et al., 2012), yielding a value similar to that determined earlier by Kleine et al. (2005); -3.47 ± 0.09 2σ. Precise W isotope compositions of iron meteorites are used to determine the timing of core formation (magmatic irons) or of metal-silicate differentiation (non-magmatic irons) in their parent bodies. Using the Allende CAI initial ε^{182}W value proposed by Burkhardt et al. (2008), the timing of core differentiation in the majority of magmatic iron meteorites has been bracketed from -2.8 to $+1.4$ Ma, since the time of formation of CAIs (Kleine et al., 2009). All of the magmatic irons are systematically biased to apparently older ages (less radiogenic initial ε^{182}W) than CAI in the compilation of Kleine et al. (2009). Average ε^{182}W for most magmatic iron meteorite groups (Qin et al., 2008b) are within error of the Allende CAI initial ε^{182}W value, with the notable exception of group IVB irons which record ε^{182}W (-3.57 ± 0.10, excluding Tlacotepec) resolvably less radiogenic than the CAI initial ε^{182}W (Burkhardt et al., 2008), and barely within error of the revised Allende CAI initial ε^{182}W (Burkhardt et al., 2012). Given the currently unsettled CAI initial ε^{182}W (Kleine et al., 2005; Humayun et al., 2007; Burkhardt et al., 2008, 2012), and that some magmatic iron meteorites formed within 1–2 Ma of CAIs (Blichert-Toft et al., 2010), iron meteorites may be expected to constrain the upper limit on the solar system initial ε^{182}W.

The ε^{182}W of iron meteorites is known to be lowered by neutron capture reactions from secondary neutrons due to cosmic-ray spallation of the iron masses during space exposure as <1 m diameter objects (Kleine et al., 2005; Markowski et al., 2006a, 2006b; Masarik, 1997; Scherstén et al., 2006). The extent of secondary neutron capture has to be precisely determined if iron meteorites are to be useful in examining either the initial ε^{182}W of the solar system or small time differences between various iron meteorite groups. The neutron fluence in an iron meteorite is not uniformly distributed but is peaked ~30–40 cm below the pre-atmospheric exposure surface (Masarik, 1997), while spallogenic nuclides (e.g. noble gases) are peaked in abundance near the original exposure surface (Ammon et al., 2009). Thus, existing noble gas measurements in iron meteorites do not provide adequate corrections for neutron capture effects on ^{182}W in iron meteorites but allow upper limits to be placed on the maximum effect on ε^{182}W (Markowski et al., 2006b; Qin et al., 2008b). Precise knowledge of the neutron capture modification of isotope ratios in iron meteorites has been limited by a lack of information on the neutron fluence experienced by an iron sample cut from a <1 m iron mass. Several elements have isotopes with high neutron capture cross-sections that function effectively as neutron dosimeters including B, Cd, Sm and Gd (e.g., Schulz et al., 2012). All of these elements are lithophile except, possibly, Cd which has been investigated in iron meteorites without definitive results (Kruijer et al., 2011).

The approach taken here has been to develop new in situ neutron dosimeters involving siderophile elements in the W–Au mass region that have a comparable response to secondary neutrons as ^{182}W so that the initial ε^{182}W of IVB irons may be determined independently from the CAI initial value (Burkhardt et al., 2008, 2012; Kleine et al., 2005). The neutron capture cross-section of ^{189}Os is comparable to that of ^{182}W, and it produces ^{190}Os, which has a low neutron capture cross-section creating a positive anomaly in ε^{190}Os (Fig. 1). This reaction was successfully exploited by Huang and Humayun (2008), and more recently by Walker (2012), who showed the presence of anti-correlated isotope anomalies in ε^{189}Os and ε^{190}Os in IVB irons with a maximum effect in Tlacotepec, the iron meteorite with the lowest ε^{182}W (-4.5 to -4.0, Horan et al., 1998; Markowski et al., 2006a, 2006b; Scherstén et al., 2006; Qin et al., 2008b). However, W isotope compositions of most of the IVB irons analyzed for Os isotopes were not available in the literature, and direct measurement of W isotopes on the same aliquots analyzed for Os isotopes is important since neutron fluence varies significantly within a single iron meteorite. Another GCR reaction that has potential for neutron dosimetry is the neutron capture of ^{191}Ir to form ^{192}Pt, since the resulting isotope has a low natural abundance (0.78%) and the large amplification of the neutron capture reaction makes this a potentially sensitive neutron dosimeter (Fig. 1).

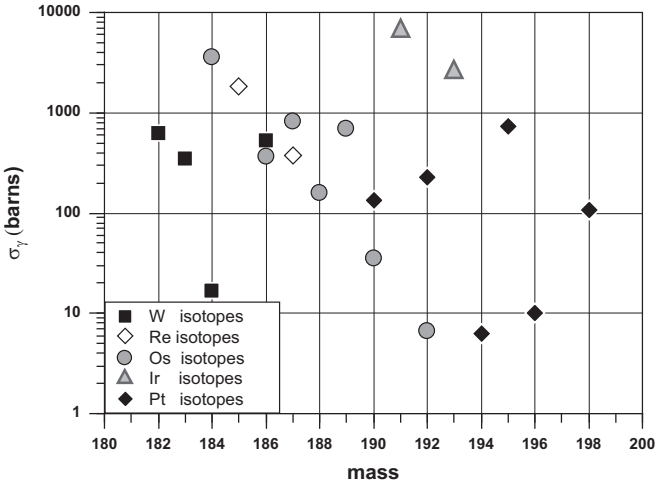

Fig. 1. Thermal neutron capture cross sections of W (black squares), Re (open diamonds), Os (grey circles), Ir (grey triangles) and Pt isotopes (black diamonds) given as $\sigma\gamma$ (barns) (Mughabghab, 2003).

In this study, we report precise isotope compositions of W, Os and Pt on 12 of the 13 known IVB iron meteorites (Tenera was not obtainable for this project). From correlations of ε^{182}W with ε^{189}Os and ε^{192}Pt, we calculate a precise and consistent value for the pre-irradiation ε^{182}W for the IVB magmatic iron meteorite group. We also confirm that there appears to be a small nucleosynthetic effect in ε^{184}W in IVB irons as reported previously (Qin et al., 2008a, 2008b). We use the Os isotope data to evaluate whether nucleosynthetic anomalies in Os isotopes are resolvable, which may be expected from the isotope anomalies observed in Mo (Burkhardt et al., 2011), Ru (Chen et al., 2010; Fischer-Gödde et al., 2012) and W (Qin et al., 2008a, 2008b) for IVB irons. This provides important constraints on the likely origins of nucleosynthetic effects in bulk iron meteorites.

2. Analytical methods

Between 0.3 and 0.9 g of 12 IVB iron meteorites were sawn from larger pieces using a jewellers' handsaw with stainless steel blades, hand-polished with Al_2O_3 sand paper to remove saw marks, rinsed with DI water and immediately digested in pre-cleaned Carius tubes with inverse Aqua Regia (iAR, HCl–HNO_3 [1:3]) (Shirey and Walker, 1995). After digestion (230 °C, >48 h), the Carius tubes were opened and Os was removed by established solvent extraction procedures (Cohen and Waters, 1996) and purified by micro-distillation prior to analysis by N-TIMS or MC-ICP-MS.

After the extraction of Os, aliquots of the sample iAR solution (~10%) were dried down and dissolved in 0.1 M HCl–0.01 M HF–1% H_2O_2 and loaded onto columns with 2 mL cation resin (AG 50W-X8 [200–400 mesh]) in order to retain Fe, Ni and other matrix cations on the column, whereas W and Pt and other anions were collected in the elutant (Puchtel and Humayun, 2001). W separation procedures were modified from Kleine et al. (2004) and Markowski et al. (2006a, 2006b). After drying down the cation column elutant, the samples were dissolved in 0.5 mL 2 M HCl-0.5 M HF and W (and Mo) was separated in 6 M HNO_3

from the remaining matrix using columns filled with anion resin (2 mL Bio-Rad^{TM} AG1-X8 [200–400 mesh]), whereas Pt was collected together with traces of Ir and Ru in 13 M HNO_3. Prior to further clean-up, the W-Mo cut was treated with $HClO_4$ to remove residual Os. After evaporation of the $HClO_4$ the samples were taken up in 0.5 M HCl–1 M HF and loaded onto a second anion column, where matrix elements were removed in 0.5 M HCl–1 M HF and 9 M HNO_3–0.01 M HF and separation of W and Mo was achieved in 7 M HCl–1 M HF and 1 M HCl, respectively.

While Ir is not an isobaric interference on Pt, the high $^{191}Ir/^{192}Pt$ and $^{193}Ir/^{192}Pt$ in these samples ranging between 21–47 and 35–81, respectively, requires efficient removal of Ir ($>98\%$) in order to eliminate large Ir beams tailing onto the 192 mass during mass spectrometry. Ir^{3+} is eluted from anion resin in high molarity HCl, and the Pt cut was boiled in 12 M HCl for approximately 24 h to achieve conversion from the 4^+-form. The samples were taken up in 0.5 M HCl–1 M HF with a trace of ascorbic acid and loaded on an anion resin column (1 mL AG1-X8 [200–400 mesh]). This clean up procedure followed the Mo and W separation scheme and Pt was again collected in 13 M HNO_3. Platinum was converted to chloride form and dissolved in 2% HCl for mass spectrometry. W and Pt yields were always higher than 85% and were monitored at each step of the clean up chemistry using a Thermo Element 2 ICP-MS.

2.1. Mass spectrometry

W, Pt and Os isotope data are reported in epsilon notation denoting the deviation of the isotope composition of W, Os or Pt in an iron meteorite from that of the terrestrial standards in parts per 10,000 according to Eq. (1),

$$\varepsilon^n A = \left[\frac{\left({}^nA/{}^mA\right)_{\text{sample}}}{\left({}^nA/{}^mA\right)_{\text{reference material}}} - 1\right] \times 10^4 \quad (1)$$

where A represents the element symbol (e.g., W, Os and Pt), and n and m are the masses of the isotopes used in the isotope ratio (e.g., $^{182}W/^{183}W$), and the reference material is the laboratory standard analyzed along with the samples. For W, NIST SRM 3163 was employed as a laboratory reference material; for Os, reagents Aristar^{TM} and HPS^{TM} were used, while for Pt, reagent HPS^{TM} Pt was used as the reference material. For the purposes of reporting isotopic deviations in non-radiogenic Os and Pt isotopes such reagent standards should suffice for present purposes, but the possibility of mass-independent isotope fractionation being widely distributed in terrestrial materials requires the development of international standards for inter-laboratory comparisons.

2.1.1. Acquisition of W, Pt and Os isotopes

All W and Pt isotope data, and some of the Os isotope data (Huang and Humayun, 2008) of the IVB irons were acquired by MC-ICP-MS using the ThermoScientific Neptune in the Plasma Analytical Facility at the National High Magnetic Field Laboratory (Florida State University, Tallahassee) during multiple analytical sessions. Additional Os isotope data were acquired by negative-ion thermal ionization mass spectrometry (N-TIMS), either at the Johnson Space Center or at the University of Houston. Precision of standard material is provided as epsilon deviation against the respective session average of the standard material. Cup configurations used during W, Os and Pt isotope data acquisition are given in Table 1.

The Neptune MC-ICP-MS sample introduction system comprised of an APEX-Q^{TM} nebulizer with a flow rate of $\sim$100 μL/min (W, Pt) or $\sim$60 μL/min (Os). Except for the Os isotope data, which were acquired using conventional Ni cones (50 V/ppm total Os), all W and Pt data were generated by using Thermo SuperJet8.0 Ni sampler cones and Spectron Ni-X skimmer cones providing a total W and Pt signal of 550 V/ppm. This configuration of the Neptune cones provides higher sensitivity, lower mass bias, and minimizes mass independent fractionation in normalized W isotope ratios (Shirai and Humayun, 2011). Each W and Pt isotope measurement given in Table A is the average of 60 ratios (1 "block"), whereas Os isotope data acquired by MC-ICP-MS is the average of 140 ratios. Integration time for W, Os and Pt isotope ratios was 4 s per peak.

For W isotopes, the samples were diluted to 25 ng/mL (2% HNO_3–trace HF). Measurements of one block were bracketed between 25 ng/mL aliquots of SRM 3163W (3–5 blocks, 2% HNO_3–trace HF) in order to monitor drift in instrumental performance. Potential isobaric interferences from ^{186}Os and ^{184}Os were monitored at ^{188}Os but chemical processing prior to mass spectrometry effectively eliminated Os from the W aliquots, thus, Os isobars were found to be at instrumental background levels and isobaric corrections were insignificant at the current level of precision. Instrumental mass bias was corrected using $^{186}W/^{183}W$ of 1.98594 (Volkening et al., 1991) using the exponential law. Measurements of $\varepsilon^{182}W$ and $\varepsilon^{184}W$ of IVB iron meteorites are accompanied by 400 W isotope measurements of SRM 3163. The typical in-session (>24 h, $n=40$–100) and long term SRM3163 reproducibility (11 analytical sessions) of $\varepsilon^{182}W$ ($\pm 0.25\varepsilon$ 2σ) and $\varepsilon^{184}W$ ($\pm 0.1\varepsilon$, 2σ) are identical.

For the determination of Pt isotopes, the Pt cut of the IVB irons was diluted to 100 ng/mL (2% HCl) to accommodate for the low natural abundance of ^{192}Pt and bracketed between 3 to 5 blocks of 100 ng/mL reagent Pt solutions (2% HCl) prepared by dilution from HPS^{TM} Pt concentration standard. Pt isotope ratios were normalized to ^{195}Pt and $^{198}Pt/^{195}Pt=0.211740$ (Rosman and Taylor, 1997) was used for mass bias corrections utilizing the exponential law. ^{189}Os and ^{199}Hg were monitored for interference

Table 1
Detector assignment used during mass spectrometry.

Isotope	Instrumentation	L4	L3	L2	L1	C	H1	H2	H3	H4	Mass bias corr.	
W	MC-ICP-MS	–	182	**183**	184	185	186	187	188	190	$^{186/183}W$	$\varepsilon^{182}W$, $\varepsilon^{184}W$
		–	W	**W**	W	Re	W	Re	Os	Os		
Os	MC-ICP-MS	182	184	186	187	**188**	189	190	192	194	$^{192/188}Os$	$\varepsilon^{189}Os$, $\varepsilon^{190}Os$
		W	Os	Os	Os	**Os**	Os	Os	Os	Pt		
Os	N-TIMS	182	184	186	187	**188**	189	190	192	194	$^{192/188}Os$	$\varepsilon^{189}Os$, $\varepsilon^{190}Os$
		W	Os	Os	Os	**Os**	Os	Os	Os	Pt		
Pt1	MC-ICP-MS	189	191	192	193	194	**195**	196	198	199	$^{198/195}Pt$	$\varepsilon^{192}Pt$, $\varepsilon^{196}Pt$
		Os	Ir	Pt	Ir	Pt	Pt	Pt	Pt	Hg		
Pt2	MC-ICP-MS	–	193	194	**195**	196	198	199	–	–	$^{198/195}Pt$	$\varepsilon^{194}Pt$
		–	Ir	Pt	Pt	Pt	Pt	Hg	–	–		

Notes: Normalizing isotopes are given in bold.

corrections on ^{192}Pt, ^{196}Pt and ^{198}Pt from ^{192}Os, ^{196}Hg and ^{198}Hg. Os was absent from most samples and where present (Santa Clara, Tawallah Valley, Warburton Range) ^{192}Os corrections contributed less than 10% to the ε^{192}Pt. Traces of Hg were detected (^{199}Hg/^{195}Pt <0.000016), which contributed less than 0.1ε to ε^{196}Pt. This level of Hg was negligible with respect to ε^{192}Pt and ε^{194}Pt. ^{193}Ir/^{192}Pt in the irons was also determined and found to range 0.4 and 8.2, which equates to the removal of 80% to 100% of the constituent Ir. Interferences from HfO+ were not monitored during analysis because IVB iron meteorites contain essentially no Hf, and all column procedures were performed on resins that were dedicated to iron meteorite matrices, exclusively. Selected sample cuts were monitored, using a Thermo Element 2 ICP-MS, for Lu and Hf which were found to be below detection limit. Reproducibilities of the HPS^{TM} Pt standard ($n=42$) for ε^{192}Pt, ε^{194}Pt and ε^{196}Pt were $\pm0.4\varepsilon$, $\pm0.5\varepsilon$ and $\pm0.1\varepsilon$, respectively.

Os isotope mass fractionation was corrected to ^{192}Os/^{188}Os$=$ 3.083 using the exponential law. After micro-distillation, aliquots of the IVB solutions were analyzed in three sessions using N-TIMS at the NASA Johnson Space Center (2008) and the University of Houston (this study), respectively, and characterized against the Houston in-house Os standard (Brandon et al., 2005) ($n=20$), which yielded a total reproducibility of $\pm0.06\varepsilon$ and $\pm0.09\varepsilon$ for ε^{189}Os and ε^{190}Os, respectively (2σ). IVB iron Os isotope data were also acquired by MC-ICP-MS as 1000 ng/mL replicates (in 5% HBr) against Aristar^{TM} ($n=2$) and HPS^{TM} Os ($n=5$) reagent standard solutions. ^{194}Pt was monitored for interference correction of ^{192}Pt from ^{192}Os using a ^{192}Pt/^{194}Pt$=$0.0237. The reproducibility of these solutions was always better than $\pm0.14\varepsilon$ and $\pm0.17\varepsilon$ (2σ) for ε^{189}Os and ε^{190}Os, respectively.

3. Results

The average values of W, Pt and Os isotope data for each of the 12 IVB iron meteorites analyzed in this study are presented in Table 2, together with the 2 standard error of the mean of the n runs ($2\sigma_m$), which is used in this contribution to signify uncertainties unless stated otherwise. The number of mass spectrometric replicate analyses performed was different for each element and is also given in Table 2. The W, Os and Pt isotope data of individual replicate measurements are provided in Table A (supplementary material) which also shows the source for each sample. The long-term ε^{182}W reproducibility of individual measurements of 60 blocks of SRM 3163 is characterized by an external precision of $\pm0.25\varepsilon$. Samples with fewer replicate analyses yield slightly lower ε^{182}W precision $>0.14\varepsilon$, whereas more thoroughly characterized irons have smaller ε^{182}W uncertainties $<0.10\varepsilon$. Notable exceptions are Iquique (-3.55 ± 0.03, $n=3$) and Cape of Good Hope (-3.68 ± 0.05, $n=2$), where the realistic errors are better represented by $\pm0.25/\sqrt{n}$.

Overall, the W isotope data are in good agreement with previously published data for IVBs (Markowski et al., 2006a, 2006b; Qin et al., 2008b; Scherstén et al., 2006). The W isotope data of the IVB irons reveal a cluster ($n=8$) around ε^{182}W$\sim-3.6\pm0.1$, with four outliers (Fig. 2). Resolved from this cluster is Tlacotepec, which has substantially lower ε^{182}W$=-4.21\pm0.13$, and the newly characterized sample Dumont, ε^{182}W$=-3.85\pm0.06$, which is intermediate between the IVBs of the cluster and Tlacotepec. Weaver Mountains (-3.33 ± 0.12) and Warburton Range (-3.42 ± 0.16) are marked by the least radiogenic ε^{182}W which distinguishes them from the cluster. The existence of the cluster in IVB ε^{182}W explains why, after exclusion of the obviously deviant Tlacotepec, an average IVB composition of -3.6 ± 0.1 was used by Burkhardt et al. (2008) to represent IVB irons. This IVB composition was well-resolved from other magmatic iron meteorites and plots to the more unradiogenic side of the CAI value (Burkhardt et al., 2008).

The variability of ε^{184}W in the IVB irons is limited but appears resolved from the terrestrial standard data with an average deficit of $-0.14\varepsilon\pm0.08\varepsilon$ based on 60 measurements (Fig. 2). This deficit is consistent with small ε^{184}W deficits in the IVB iron meteorites

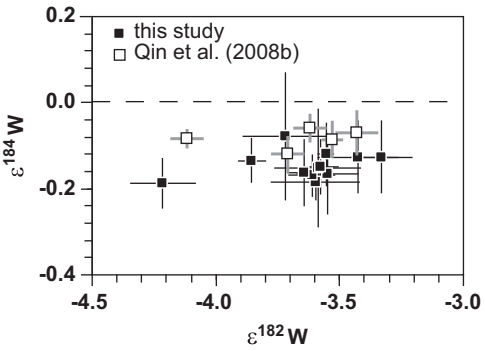

Fig. 2. Comparison of ε^{184}W and ε^{182}W of IVB irons from this study (black squares) and literature values (open squares, Qin et al., 2008a, 2008b). Uncertainties are given as 2se$_m$.

Table 2
W, Os and Ir-Pt isotope data of IVB iron meteorites.

	ε^{182}W	2se$_m$	ε^{184}W	2se$_m$	n	ε^{189}Os	2se$_m$	ε^{190}Os	2se$_m$	n	raw ratios		ε^{192}Pt	2σ	ε^{192}Pt$_{Ir}$	ε^{194}Pt	2σ	ε^{196}Pt	2σ
											^{193}Ir/^{192}Pt	^{193}Ir/^{195}Pt	meas.		corr.				
Cape of Good Hope	−3.60	0.18	−0.13	0.10	3	−0.32	0.11	0.11	0.06	4	8.23	0.19	26.7	0.8	24.6	1.01	0.10	0.27	0.19
Dumont	−3.85	0.06	−0.13	−0.13	9	−0.23	0.07	0.26	0.01	2	2.67	0.06	24.3	0.3	23.6	0.89	0.11	0.42	0.08
Hoba	−3.61	0.09	−0.17	0.05	8	−0.06	0.03	0.00	0.00	4	0.47	0.01	13.8	0.4	13.7	0.29	0.11	0.19	0.11
Iquique	−3.55	0.03	−0.12	−0.12	3	−0.25	0.05	0.18	0.03	3	4.61	0.11	25.4	1.0	24.3	0.91	0.11	0.03	0.24
Kokomo	−3.55	0.12	−0.16	0.04	3	−0.25	0.06	0.15	0.03	5	0.45	0.01	31.9	0.8	31.8	0.61	0.12	0.22	0.19
Santa Clara	−3.64	0.06	−0.16	−0.16	5	−0.34	0.01	0.14	0.10	2	2.65	0.06	14.4	0.4	13.8	0.96	0.11	0.04	0.09
Skookum	−3.59	0.17	−0.15	0.13	3	−0.16	0.00	0.19	0.03	2	4.10	0.09	7.3	0.6	6.3	−0.32	0.12	−0.11	0.09
Tawallah Valley	−3.72	0.17	−0.08	0.15	2	−0.24	0.10	0.06	0.05	4	0.64	0.01	8.8	0.5	8.6	0.28	0.10	−0.20	0.11
Tinnie	−3.57	0.07	−0.15	0.06	9	−0.05	0.03	0.03	0.02	1	0.46	0.01	6.4	0.3	6.3	0.12	0.10	0.15	0.08
Tlacotepec	−4.21	0.13	−0.18	0.06	3	−0.64	0.06	0.39	0.07	4	0.81	0.02	53.0	0.4	52.8	1.54	0.10	0.73	0.08
Weaver Mountains	−3.33	0.12	−0.12	0.08	6	−0.03	0.01	0.06	0.03	2	0.61	0.01	4.4	0.3	4.4	0.17	0.11	0.13	0.07
Warburton Range	−3.42	0.16	−0.12	0.08	6	0.02	0.06	0.05	0.08	2	6.33	0.15	7.5	0.5	5.9	−0.06	0.07	−0.09	0.13

Notes: Epsilon notation given as deviation in parts of 10,000 from terrestrial standards. Uncertainties of all W and Os isotope data are given as standard error of the mean (2se$_m$) derived from replicate measurements of the same digestions (n). Uncertainties of Pt isotopes are given as in-run standard deviation (2σ).

observed by Qin et al. (2008a, 2008b), who attributed this to a nucleosynthetic effect. There appears to be no correlation between ε^{184}W and ε^{182}W (Fig. 2) or ε^{192}Pt indicating that cosmogenic effects are negligible consistent with the ε^{184}W being a nucleosynthetic anomaly.

Fig. 3 shows the Pt isotope data for IVB irons compared with predictions from a cosmogenic production model. The range of ε^{192}Pt, ε^{194}Pt and ε^{196}Pt in the IVB iron meteorites extends from $+4.4$ to $+53$, -0.32 to $+1.54$ and -0.20 to $+0.73$, respectively (Fig. 3). All ε^{192}Pt values of these irons are positive and well resolved from the terrestrial standard. The ε^{192}Pt and ε^{194}Pt deviation of IVB iron meteorite from the terrestrial standards is most pronounced in Tlacotepec ($+53\varepsilon$), whereas Weaver Mountains and Warburton Range show the smallest offset. The remaining samples have Pt isotope systematics between Tlacotepec and Weaver Mountains. In ε^{192}Pt–ε^{194}Pt space, the IVB irons are positively correlated, although some scatter is apparent (Fig. 3). These data are in good agreement with model predictions for galactic cosmic ray (GCR) effects. In ε^{192}Pt–ε^{196}Pt space the IVBs are also correlated but the magnitude of the variation is lower, with Tlacotepec being distinct from the other IVB irons (0.73ε). The change in ε^{196}Pt is produced exclusively by neutron capture on ^{195}Pt, and is independent of the Ir/Pt ratio of the meteorite, which varies by about a factor of 2 in these irons (Campbell and Humayun, 2005; Walker et al., 2008). However, the ε^{192}Pt is dependent on the Ir/Pt ratio. This dependence is not apparent in Fig. 3A because both ε^{192}Pt and ε^{194}Pt are similarly dependent on the Ir/Pt ratio. Thus, in Fig. 3B, the distinct predictions of the nuclear model for neutron capture effects appear as two limits, the lower limit that of the high Ir/Pt irons exemplified by Cape of Good Hope, and the upper limit that of low Ir/Pt irons exemplified by Warburton Range. The fact that most of the IVBs follow the Cape of Good Hope compositional line is due to the higher neutron dosages experienced by the least fractionated IVB irons (Ir/Pt$\sim$1), particularly Tlacotepec (Fig. 3B).

Fig. 4A shows the effect of deliberately adding Ir to an aliquot of HPS^{TM} Pt standard solution. There is an apparent increase in the ε^{192}Pt due to peak tailing from ^{191}Ir and ^{193}Ir that flank the ^{192}Pt peak (Table 1). The inset in Fig. 4A shows that the Ir memory effect is trivial for the purposes of these measurements. Fig. 4B shows the ε^{192}Pt for IVB irons plotted against the $(^{193}\text{Ir}/^{195}\text{Pt})_{raw}$ ratio. Both corrected and uncorrected data are given in Table 2, and shown in Fig. 3. The maximum correction applied is 2ε units for Cape of Good Hope, and $\sim 1\varepsilon$ units for Iquique and Skookum, with the remaining samples having corrections that are comparable to or smaller than the analytical errors. The extent of the correction implies an abundance sensitivity of about 20 ppm for the Neptune in the Ir–Pt mass range. Peak tailing effects are negligible on ^{194}Pt because of its higher intensity, e.g., $(^{193}\text{Ir}/^{195}\text{Pt})_{raw} < 0.19$, and so no corrections were applied to ε^{194}Pt.

The Os isotope data of the IVB irons are shown in Fig. 5 where ε^{189}Os anti-correlates with ε^{190}Os. This figure also reveals a cluster

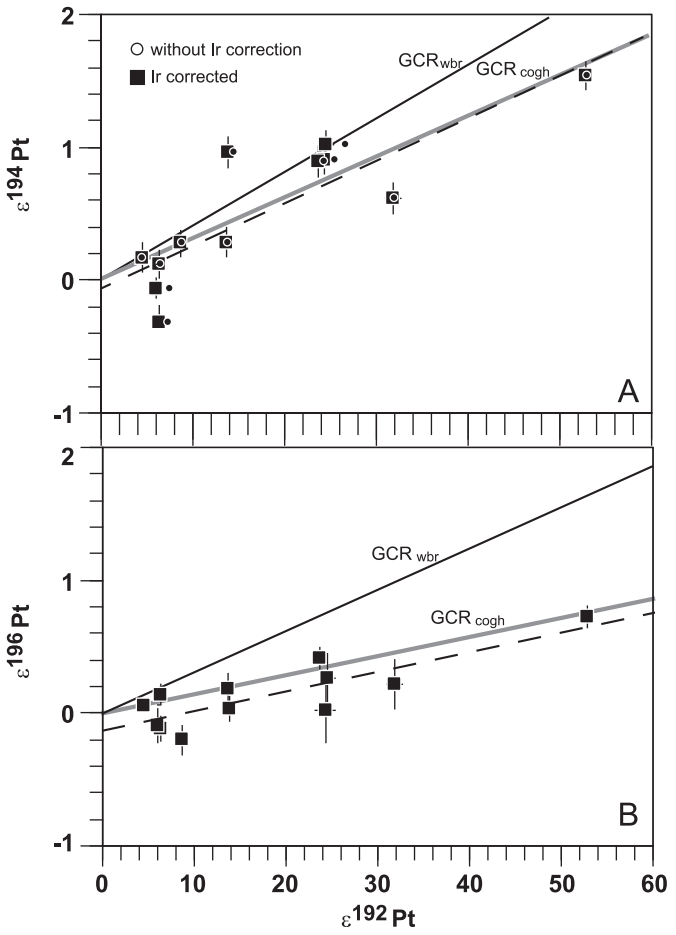

Fig. 3. Comparison of ε^{194}Pt (A) and ε^{196}Pt (B) against ε^{192}Pt. Here, and elsewhere, ^{195}Pt is the denominator isotope. In panel (A), Os- and Hg-interference corrected data are given with (black squares) and without (black circles) Ir-tailing corrections. A linear regression line (dashed) through the data is shown. Uncertainties are given as $2\sigma_m$. The Pt isotope variation predicted by the nuclear model due to GCR reactions for compositions of Cape of Good Hope (thick grey line, GCRcogh) and Warburton Range (thin black line, GCRwbr), the two compositional extremes, is also provided.

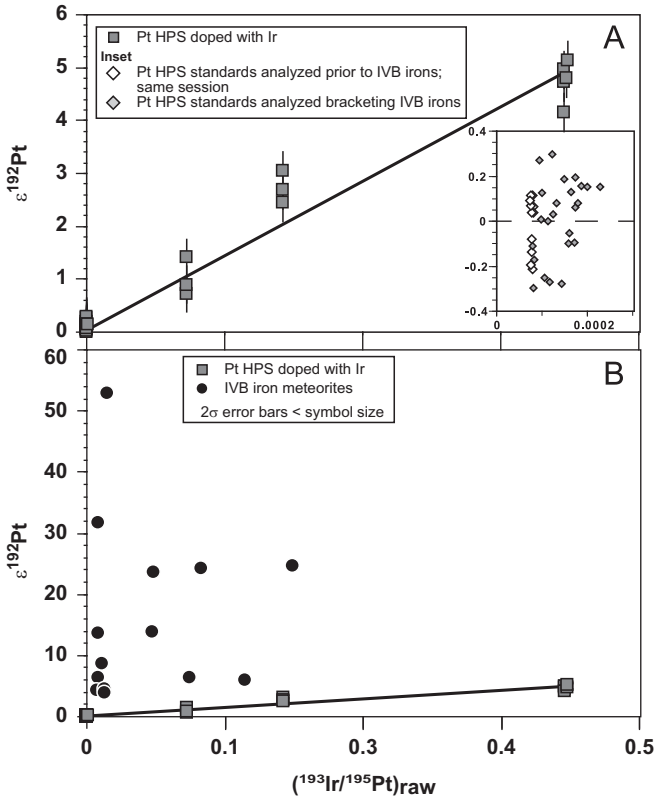

Fig. 4. Panel (A) shows the effect of Ir tailing parameterised as $(^{193}\text{Ir}/^{195})$raw during mass spectrometry on ε^{192}Pt of Ir-doped HPS Pt standard solution (grey squares), together with pure HPS Pt standards run prior to introduction of IVB irons (open diamonds) and those bracketing the samples (grey diamonds). In panel (B), the extent of Ir correction on the IVB irons can be assessed by comparing the ε^{192}Pt and $(^{193}\text{Ir}/^{195})$raw of Ir-doped HPS Pt standard solutions with that of the IVB iron meteorites (black circles). Samples that require essentially no correction plot near the y-axis.

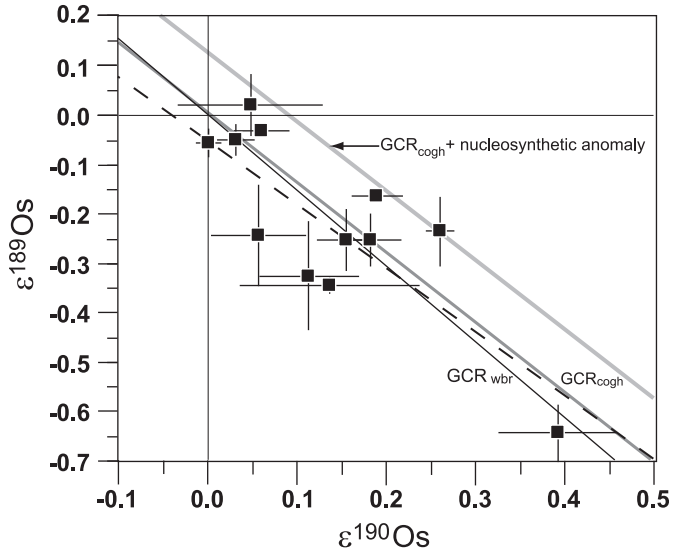

Fig. 5. ε^{189}Os vs. ε^{190}Os of the IVB irons is shown together with the predictions of a nuclear model for GCR reactions on the compositions of Cape of Good Hope (thick grey line, GCRcogh) or Warburton Range (thin black line, GCRwbr). A linear regression line (dashed) through the data is shown. Uncertainties are given as $2se_m$. Also shown is the nuclear model prediction for Cape of Good Hope if a small nucleosynthetic effect on ε^{189}Os ($+0.17\varepsilon$, thick light grey line) is assumed.

($n=5$) with slight ^{189}Os deficit/ε^{190}Os excess ($\varepsilon^{189}\text{Os} = -0.26 \pm 0.08\varepsilon$; $\varepsilon^{190}\text{Os} = +0.17 \pm 0.06\varepsilon$, Fig. 5) relative to terrestrial standards. Tlacotepec ($\varepsilon^{189}\text{Os} = -0.64\varepsilon$; $\varepsilon^{190}\text{Os} = +0.39\varepsilon$) and Dumont have stronger ^{189}Os deficit/ε^{190}Os excesses whereas Hoba, Warburton Range, Tinnie and Weaver Mountains are identical within analytical uncertainty ($^{189}\text{Os} = -0.03 \pm 0.06$; $^{190}\text{Os} = +0.03 \pm 0.06$, 2σ) with the terrestrial value.

4. Discussion

4.1. Isotope systematics and relevant neutron capture reactions in the mass range between W and Au

Iron meteorites have experienced an extended period of exposure to GCR ranging from a few Ma to over 2000 Ma (Eugster, 2003; Herzog, 2007; Lavielle et al., 1999; Voshage, 1984; Voshage and Feldmann, 1979). Primary GCRs produce secondary neutrons in iron meteorites and these neutrons are captured by siderophile element nuclei transmuting them (Leya et al., 2003; Masarik, 1997). This is a particular concern for ε^{182}W, since ^{182}W is the first major nuclide in the W-Au mass region and it has no source for production; it is simply destroyed by neutron capture resulting in cosmogenic burn-out of ^{182}W (Leya et al., 2003; Masarik, 1997). W isotope chronology of the early solar system is impacted by the GCR reactions (Markowski et al., 2006a; Qin et al., 2008b) given in reaction 1,

$$^{182}\text{W} + \text{n} \rightarrow {}^{183}\text{W}$$
$$^{183}\text{W} + \text{n} \rightarrow {}^{184}\text{W}$$
$$^{185}\text{Re} + \text{n} \rightarrow {}^{186}\text{Re(EC)} \rightarrow {}^{186}\text{W}$$
$$^{186}\text{W} + \text{n} \rightarrow {}^{187}\text{W}(\beta^-) \rightarrow {}^{187}\text{Re} \qquad \text{(reaction1)}$$

Aside from W, the isotopic changes induced in other nuclei in the W–Au region have not been explored previously. For this study, we have calculated a detailed neutron capture model for nuclei in the W–Au region for meteoroids ranging in size from 10–120 cm modifying an earlier model for the calculation of nuclide production rates from charged particle capture (Ammon et al., 2009). Details of this model are provided in the supplementary material.

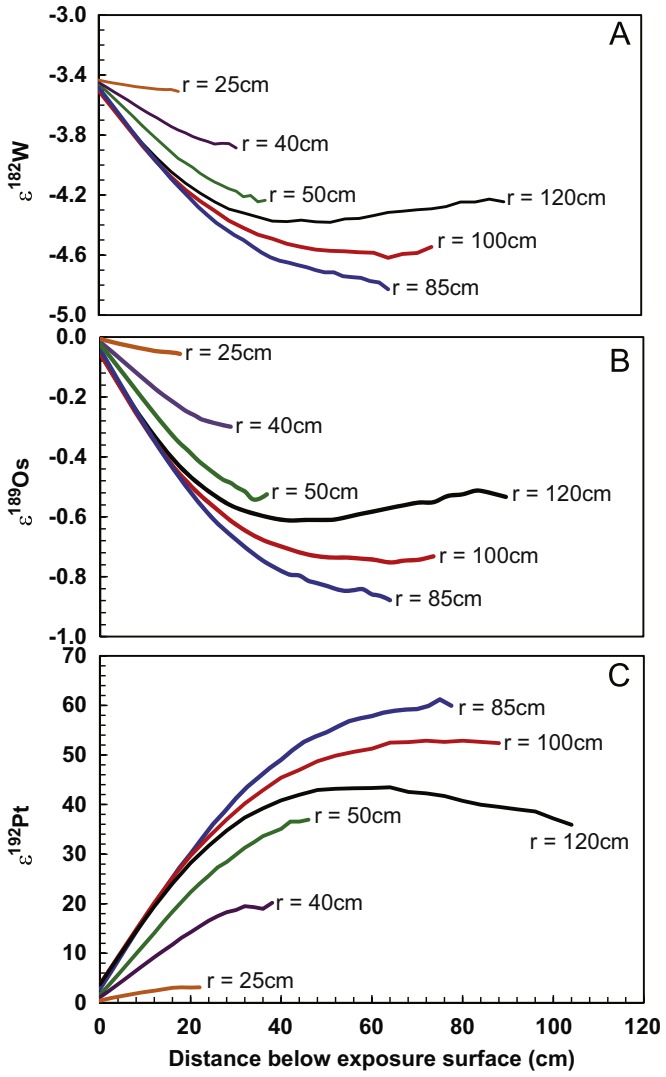

Fig. 6. Nuclear model predictions of the effects of secondary neutron capture on the isotopes of W, Os and Pt as a function of depth below the exposure surface for iron meteoroids of different radii: 25 cm (orange), 40 cm (violet), 50 cm (green), 85 cm (blue), 100 cm (red) and 120 cm (black). A. ε^{182}W; B. ε^{189}Os; C. ε^{192}Pt. The maximum effects for all three isotopes occur in the center of an 85 cm body, and the effects diminish again with increasing radius. The neutron mean free path is ~10 cm in iron meteorites so that the smallest bodies ($r < 25$ cm) lose neutrons to space before capture reactions can occur on the nuclei of trace elements like W, Os and Pt. (For interpretation of the references to color in this figure legend, the reader is referred to the web version of this article.)

Fig. 6 uses this model to predict ε^{182}W as a function of depth from the surface and meteoroid size, assuming an initial $\varepsilon^{182}\text{W} = -3.42$ and an exposure age of 945 Ma relevant for Tlacotepec (Voshage and Feldmann, 1979; Voshage, 1984). For bodies smaller than 25 cm, the cosmogenic burn-out of ε^{182}W is < 0.1. The cosmogenic burn-out increases with depth and reaches a maximum effect ($\varepsilon^{182}\text{W} = -4.8$) for 65–85 cm bodies, and then gradually diminishes in larger bodies (100–120 cm) due to increased shielding. This model predicts little influence of secondary neutrons on the ε^{184}W ($< 0.03\varepsilon$). The effect on W is largely controlled by the neutron energy distribution and is nearly independent of chemical composition of the iron meteoroid; the exception is the branching decay of ^{186}Re which decays by electron capture to ^{186}W (7%) (reaction (1)) and ^{186}Os (93%),

and has a negligible influence (0.02ε) on the ε^{182}W via its impact on the normalizing ^{186}W/^{183}W ratio.

In the case of Os isotopes, the neutron capture reaction given in reaction (2) is utilized to characterize the effects of GCR.

$$^{189}\mathrm{Os} + \mathrm{n} \rightarrow {}^{190}\mathrm{Os} \qquad \text{(reaction2)}$$

Here ^{190}Os, which has a relatively insignificant cross section, accumulates the burn-out signal from ^{189}Os. The even Os isotopes (excluding ^{184}Os) have lower neutron capture cross sections (σ_γ) than the odd Os isotopes (Fig. 1), so that normalization to ^{192}Os/^{188}Os is not compromised by cosmogenic neutron capture. The situation for ε^{189}Os is very similar to that for ε^{182}W (Fig. 6) with the maximum extent of ^{189}Os burn-out occurring in 65–85 cm bodies ($\varepsilon^{189}\mathrm{Os} = -0.9$) being only slightly smaller than the comparable effect in ε^{182}W (a relative change of -1.4). The model predicts an anti-correlation between ε^{189}Os and ε^{190}Os (Fig. 5) with a weak dependence on the chemical composition (Re/Os and Ir/Os ratios) due to neutron capture on ^{187}Re forming ^{188}Os, and neutron capture on ^{191}Ir which decays by an electron capture branch (5%) to ^{192}Os. These effects are propagated to the other isotopes by mass bias correction using the ^{192}Os/^{188}Os ratio. This dependence on chemical composition is shown in Fig. 5 by two model curves representing the end member compositions of Cape of Good Hope (Re/Os = 0.067, Ir/Os = 0.64) and Warburton Range (Re/Os = 0.083, Ir/Os = 0.92).

Platinum has six isotopes, including four high abundance isotopes (^{194}Pt [32.9%], ^{195}Pt [33.8%], ^{196}Pt [25.3%], ^{198}Pt [7.2%]) generated predominantly by the r-process, and two low abundance isotopes, p-process ^{190}Pt [0.01%] and s-process ^{192}Pt [0.79%]. Neutron capture reactions pertaining to Pt isotopes involve Ir (reactions (3) and (4)) as well as higher mass Pt isotopes (reactions (5) and (6)).

$$^{191}\mathrm{Ir} + \mathrm{n} \rightarrow {}^{192}\mathrm{Ir}(\beta^-) \rightarrow {}^{192}\mathrm{Pt} \qquad \text{(reaction3)}$$

$$^{193}\mathrm{Ir} + \mathrm{n} \rightarrow {}^{194}\mathrm{Ir}(\beta^-) \rightarrow {}^{194}\mathrm{Pt} \qquad \text{(reaction4)}$$

$$^{194}\mathrm{Pt} + \mathrm{n} \rightarrow {}^{195}\mathrm{Pt} \qquad \text{(reaction5)}$$

$$^{195}\mathrm{Pt} + \mathrm{n} \rightarrow {}^{196}\mathrm{Pt} \qquad \text{(reaction6)}$$

Neutron capture on ^{191}Ir, the nuclide with the largest σ_γ in the W–Au region, produces ^{192}Ir which decays via β^- to ^{192}Pt with a branching decay (95%), and this is a prominent effect. Fig. 6 shows the accumulation of ε^{192}Pt expected for a IVB iron with the composition of Cape of Good Hope (Ir/Os = 1.03), with the effect being a factor of two smaller for Warburton Range (Ir/Os = 0.46). Neutron capture on ^{193}Ir forms ^{194}Pt, but due to the higher natural abundance of ^{194}Pt, the maximum $\varepsilon^{194}\mathrm{Pt} = 1.5$ for Cape of Good Hope, with a similar dependence on Ir/Pt ratio. The neutron capture of ^{195}Pt to ^{196}Pt is not dependent on the chemical composition since the normalizing isotopes (^{195}Pt and ^{198}Pt) are not produced by reactions on any other element. The maximum $\varepsilon^{196}\mathrm{Pt} = 0.9$ in the center of an 85 cm body is similar to the effect in ε^{189}Os.

The size of the parent meteoroid and the depth of burial of five of the IVB irons were estimated from ^{41}K–^{40}K dating (Voshage, 1984; Voshage and Feldmann, 1979). Comparing with new measurements of ε^{192}Pt for these irons and the model presented above, using published Ir/Pt ratios (Campbell and Humayun, 2005; Walker et al., 2008), we find that Cape of Good Hope and Hoba agree reasonably well with the earlier estimates of size and depth. However, Skookum, Tlacotepec and Weaver Mountains require larger bodies (>40 cm; >65 cm; >50 cm, respectively). The largest effect in ε^{192}Pt is observed in Tlacotepec (53ε) requiring burial in the center of a 65 cm body, or 44–50 cm burial depth in an 85 cm body (Fig. 6), compared with 34 cm burial depth in a 45 cm body previously estimated (Voshage, 1984).

4.2. Pre-GCR ε^{182}W derived from correlated W–Os–Pt isotope systematics

The W isotope data set of the group IVB irons is the most extensive of its kind yet published. One advantage of this comprehensive approach to sample coverage is that it is now apparent that IVB irons exhibit a wider range of ε^{182}W than previously recognized (Markowski et al., 2006a, 2006b; Qin et al., 2008b; Scherstén et al., 2006). The newly characterized samples Iquique, Kokomo and Tinnie have ε^{182}W akin to the majority of previously characterized samples, whereas Weaver Mountains has the highest ε^{182}W (-3.35 ± 0.12) among these irons similar to Warburton Range (-3.42 ± 0.16) and within error of the most recent CAI values, -3.28 ± 0.12 and -3.51 ± 0.10 (Burkhardt et al., 2008, 2012). Qin et al. (2008b) adopted two approaches to recognizing cosmogenic effects in irons, (i) the irons with the lowest ε^{182}W were corrected for the maximum cosmogenic effect which was then taken as an upper bound on the pre-irradiation ε^{182}W, and (ii) the irons with the highest ε^{182}W were taken as the lower bound on the pre-irradiation ε^{182}W. Adopting their second approach here, we average the ε^{182}W of Weaver Mountains and Warburton Range to obtain the lower bound of the pre-irradiation ε^{182}W of the IVB irons as -3.39 ± 0.10 in contrast to -3.48 ± 0.02 (Qin et al., 2008b).

Cosmogenic noble gas signatures were previously used to assess GCR effects in iron meteorites using correlations between ^{3}He abundances and ε^{182}W (Markowski et al., 2006a, 2006b). These correlations showed that the W isotope variation of IVB irons in the range of ε^{182}W -3.3 to -4.3 does not reflect chronological information. Although the co-variation of noble gas – ε^{182}W has been used for GCR correction (Markowski et al., 2006a), the pre-irradiation ε^{182}W group average (-3.6 ± 0.1) remained resolved from the CAI initial ε^{182}W of Burkhardt et al. (2008) but indistinguishable from the revised CAI initial ε^{182}W of Burkhardt et al. (2012).

In this study, in situ neutron dosimeters based on stable Os and Pt isotope systematics are coupled to ε^{182}W measured on the same sample. In Fig. 7, the ε^{182}W data determined in this study show a correlation with ε^{189}Os, ε^{190}Os and ε^{192}Pt with Tlacotepec and Weaver Mountains representing the two extremes. The dashed black line in Fig. 7 is a linear regression fit to the correlation. Back-projection of the linear regression to the pre-irradiated Pt and Os isotopic compositions, here assumed to be 0-epsilon, indicates pre-GCR irradiation values of ε^{182}W of -3.42 ± 0.15 (2σ, ε^{192}Pt), -3.43 ± 0.14 (2σ, ε^{190}Os) and -3.42 ± 0.12 (2σ, ε^{189}Os). The ε^{189}Os and ε^{190}Os anomalies result from the same neutron capture reaction (reaction (2)) and are treated here as two measurements of the same quantity, yielding the average Os-derived ε^{182}W intercept -3.43 ± 0.09 (2σ). Combining the average ε^{182}W acquired in this manner from the Os–W correlation with that obtained from the Pt–W correlation, the average pre-irradiation ε^{182}W of the group IVB iron meteorites is -3.42 ± 0.09 (2σ). The value of -3.42 ± 0.09 (2σ) representing the complete dataset agrees well with the average value of ε^{182}W (-3.39 ± 0.10, 2σ) for the two least irradiated IVB irons. Both values of ε^{182}W are within error of the new CAI initial $\varepsilon^{182}\mathrm{W} = -3.51 \pm 0.10$ (Burkhardt et al., 2012). In the first few million years (Ma) of solar system history, the rate of ε^{182}W evolution is $\sim 0.10\varepsilon$/Ma. Thus, the time difference represented by the pre-irradiation IVB iron initial ε^{182}W (-3.42 ± 0.09, 2σ) and the CAI initial ε^{182}W (-3.51 ± 0.10; Burkhardt et al., 2012) is $+0.9 \pm 1.3$ Ma.

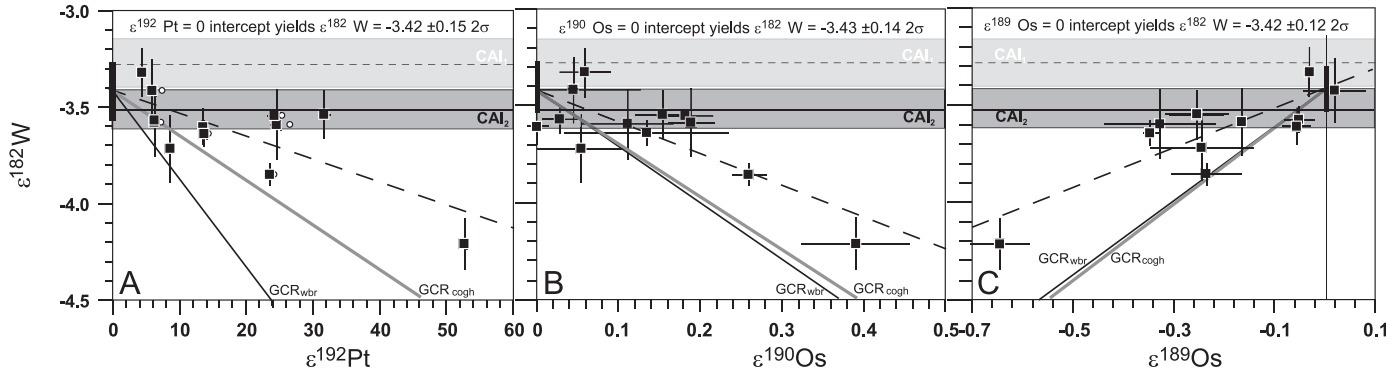

Fig. 7. Correlation of ε^{182}W with in situ neutron dosimeters in IVB iron (A) ε^{192}Pt, (B) ε^{189}Os, and (C) ε^{190}Os. Data were generated from the same digestions (W, Os and Pt isotopes) or from the same sample stock (Os isotopes, ca. 1 cm^3) and Ir-corrected (black squares) and Ir-uncorrected ε^{192}Pt (open circle) are shown in panel (A). Uncertainties are given as $2se_m$ (W and Os isotopes) and 2σ (Pt isotopes). The grey bands show the ε^{182}W of the two most recent CAI initial determinations (CAI1, $-3.28 \pm 0.12\varepsilon$, Burkhardt et al., 2008 and CAI2, $-3.51 \pm 0.10\varepsilon$, Burkhardt et al., 2012). In each panel, a dashed linear regression line is shown projecting at the x-axis intercept of 0 yielding the pre-GCR ε^{182}W of the IVB iron meteorite group (black bar, 2σ). The isotope correlation predicted by the nuclear model due to GCR reactions for compositions of Cape of Good Hope (thick grey line, GCRcogh) and Warburton Range (thin black line, GCRwbr), the two compositional extremes, are also provided.

4.3. Comparison between nuclear models and empirical correlations

Figs. 3, 5 and 7 show the correlations predicted by the nuclear model employed here and the empirical correlation defined by the data. Since the nuclear model prediction depends on the chemical composition, two end member compositions, for the high Ir/Pt end represented by Cape of Good Hope, and for the low Ir/Pt end represented by Warburton Range, have been used. In Fig. 3, the correlation between ε^{192}Pt and ε^{194}Pt is well represented by the nuclear model, where it depends weakly on Ir/Pt ratio and on the exposure age. The model outputs were calculated for Tlacotepec with an exposure age of 945 Ma (Voshage, 1984). The correlation between ε^{192}Pt and ε^{196}Pt is strongly dependent on the Ir/Pt ratio but Tlacotepec is represented accurately by the nuclear model for the Cape of Good Hope composition, since it shares the high Ir/Pt ratio of Cape of Good Hope. In Fig. 5, good agreement is observed for the correlation between ε^{189}Os and ε^{190}Os, and the correlation is weakly dependent on the Re/W ratio. In Fig. 7, the agreement between model predictions and data is poorer for correlations between ε^{182}W and the three in situ neutron dosimeters and compositional dependence is not the issue here. The nuclear model over-predicts the extent of ε^{182}W burn-out (-4.6 vs. -4.25). The cause of the discrepancy is not known. Redetermination of the neutron capture cross sections of the W isotopes, particularly of ^{182}W, will be a first step towards resolving this discrepancy. The discrepancy between nuclear models and empirical correlations demonstrates the value of employing empirical corrections by in situ neutron dosimeters vs. exclusive dependence on the nuclear models, which together with spallogenic noble gases were the only tools available prior to this study.

4.4. Evidence for nucleosynthetic effects in W, Os and Pt isotopes in IVB irons

Nucleosynthetic anomalies in bulk chondrites and their acid leachates, and in differentiated meteorites, have been observed in Mo and Ru with carbonaceous chondrites and IVB irons showing systematic r-process excesses or s-process deficits (Burkhardt et al., 2011; Chen et al., 2010; Dauphas et al., 2002a, 2002b; Yin et al., 2002). In contrast, Brandon et al. (2005) showed that Os isotope anomalies were restricted to acid leachates of bulk chondrites and that there were no nucleosynthetic anomalies in bulk chondrites. This was confirmed by subsequent work (Reisberg et al., 2009; van Acken et al., 2011; Walker, 2012; Yokoyama et al., 2007, 2010). Irisawa et al. (2009) reported $\varepsilon^{184}W = -0.39 \pm 0.14$ for multiple measurements of the Allende CV3 chondrite, but could not resolve the effect in another CV3 chondrite, or in other carbonaceous chondrites. Qin et al. (2008a, 2008b) reported $\varepsilon^{184}W = -0.08 \pm 0.01$ (2σ) in their IVB average ($n=6$). Both these effects were attributed to a nucleosynthetic effect. In this study, the presence of a nucleosynthetic anomaly in ε^{184}W from IVB irons is clearly shown by the data in Fig. 2. All irons, including the least irradiated members of IVB, Warburton Range and Weaver Mountains, record an ε^{184}W of -0.14 ± 0.06 (2σ). This result complements the determinations of Mo (Burkhardt et al., 2011; Dauphas et al., 2002b) and Ru (Chen et al., 2010; Fischer-Gödde et al., 2012) isotope anomalies in IVBs.

Are there nucleosynthetic anomalies in Os and Pt isotopes? For Pt isotopes, this is difficult to determine in the IVB irons since the s-only isotope, ^{192}Pt, is dominated by GCR burn-out of ^{191}Ir, and the remaining isotopes are dominated ($>95\%$) by the r-process peak centered at ^{195}Pt (Arlandini et al., 1999), and have ε-level contributions from secondary neutron capture. [The p-process ^{190}Pt (0.013%) was not determined here.]

The expected nucleosynthetic isotopic anomalies in W, Os and Pt isotopes were calculated by recombining the s-process and r-process abundances with a small deficit of s-process and then comparing the resulting ratios against solar system abundances using data from Arlandini et al. (1999) with updated cross-sections for the s-process (Bao et al., 2000; Humayun and Brandon, 2007). The s-process deficit (1.7ε) was selected to yield isotope anomalies in Mo and Ru that agreed with observed IVB iron anomalies (Burkhardt et al., 2011; Chen et al., 2010). The expected effect in ε^{184}W (-0.31) is twice as large as that observed here. A small positive effect ($+0.17$) is predicted in ε^{189}Os. Fig. 5 shows a model curve featuring a cosmogenic deficiency in ε^{189}Os anti-correlated with ε^{190}Os that originates from the calculated nucleosynthetic anomaly. This curve is displaced from the measured data indicating that an isotope anomaly of the magnitude predicted is not present in ε^{189}Os. An average of the four least irradiated IVB irons (Table 2) yields $\varepsilon^{189}Os = -0.03 \pm 0.08$ (2σ), inconsistent with an anomaly even half the magnitude of the predicted anomaly. We conclude that an r-process excess or s-process deficit of the kind observed in ε^{184}W is absent in ε^{189}Os. The predicted effect in ε^{192}Pt is -1.6ε which cannot be observed in the present data since all the IVBs show small positive ε^{192}Pt effects due to cosmogenic isotope effects. Moving the ε^{192}Pt intercept from 0 to -1.6 has little impact on the GCR-corrected ε^{182}W (0.02ε). The predicted effect on ε^{194}Pt (-0.03) is negligible, and the predicted effect on ε^{196}Pt (-0.15) is near the detection limit of the current set of

measurements (Table 2). The intercept of ε^{196}Pt in Fig. 3 is -0.11 ± 0.15 (2σ); the average ε^{196}Pt of the five samples with ε^{192}Pt < 10 is -0.02 ± 0.30 (2σ), both of which just fall short of resolving the effect. The impact of the ε^{184}W anomaly observed on the ε^{182}W is negligible (Qin et al., 2008a, 2008b). The absence of observable Os isotope anomalies in bulk chondrites and iron meteorites argues against large-scale Os nucleosynthetic anomalies in the solar nebula, a conclusion also reached by Walker (2012). Instead selective inheritance of isotopic anomalies due to nebular processing of the presolar dust and/or disequilibrium melting of an isotopically heterogeneous "chondritic" precursor provide alternative mechanisms to induce the observed isotopic anomalies in Mo, Ru and W.

5. Conclusions

This study presents new W, Os, and Pt isotope data for 12 of the 13 known IVB iron meteorites and establishes correlations between ε^{182}W and ε^{189}Os and ε^{192}Pt, which are used as in situ neutron dosimeters. The largest cosmogenic neutron capture effect is observed in ε^{192}Pt where all IVBs show some effect ($>4\varepsilon$) while Tlacotepec exhibits the largest effect (53ε). By comparison, the range in ε^{189}Os is $\sim 0.6\varepsilon$, and the variation in ε^{182}W within the IVB group is $\sim 0.9\varepsilon$ making ε^{192}Pt a very sensitive indicator of cosmogenic neutron dosage in high Ir/Pt iron meteorites.

The two least irradiated IVB irons (Weaver Mountains, Warburton Range) yield ε^{182}W$= -3.39 \pm 0.10$, within error of the currently accepted initial ε^{182}W of Allende CAIs. Correlations between in situ neutron dosimeters and ε^{182}W for the IVB irons yield an initial ε^{182}W=-3.42 $\pm$ 0.15 (2σ) from ε^{192}Pt; ε^{182}W= -3.43 $\pm$ 0.14 (2σ) from ε^{190}Os; and ε^{182}W$= -3.42 \pm 0.12$ (2σ) from ε^{189}Os. The three values of initial ε^{182}W are mutually consistent and are averaged to yield a pre-irradiation ε^{182}W$= -3.42 \pm 0.09$ (2σ) for the IVB irons. After cosmogenic correction, this value of ε^{182}W is higher than the recent CAI initial of -3.51 ± 0.10 by $\sim 2\sigma$, corresponding to an age difference of $+0.9 \pm 1.3$ Ma.

A nuclear spallation model provides reasonable agreement with the empirical neutron dosimeters for intra-element isotope variation, but over-predicts the ε^{182}W burn-out by a factor of about two for reasons that need to be explored further. This establishes the value of empirical neutron dosimeters for estimating pre-irradiation ε^{182}W. The nuclear model provides estimates of the depths and sizes of the meteoroids from which the IVB irons were derived that agree for Cape of Good Hope and Hoba with previous work using ^{41}K–^{40}K dating and spallogenic noble gases (Voshage, 1984), but requires deeper burial in larger bodies than predicted by published models for Skookum, Tlacotepec and Weaver Mountains.

This study confirms the presence of small negative anomalies resolved in ε^{184}W (-0.14 ± 0.06, 2σ) in IVB irons, similar to results from Qin et al. (2008a, 2008b). The presence of nucleosynthetic effects in Mo and Ru in IVB irons (Chen et al., 2010; Burkhardt et al., 2011; Fischer-Gödde et al., 2012) indicates that the effect in ε^{184}W is likely due to nucleosynthesis, and shows no correlation with ε^{182}W or ε^{192}Pt from cosmogenic processes. If this was caused by s-process deficit inherited from an heterogeneous solar nebula, then the predicted variations in ε^{189}Os ($+0.17$) are not found in our study, nor in that of Walker (2012), while predicted effects in Pt isotopes are not resolved from cosmogenic spallation effects at the current level of precision. Possible mechanisms giving rise to such isotopic anomalies in Mo, Ru and W, but not in Os, involve disequilibrium melting of isotopically heterogeneous precursors, and/or nebular processing of pre-solar grains.

Acknowledgments

This study was funded by NASA Grant no. NNX10AI37G (M. Humayun), NNX12AD06G (A.D. Brandon), and by the Swiss National Science Foundation (I. Leya). We thank the following for kindly providing samples: Glenn MacPherson, Tim McCoy and Linda Welzenbach, Smithsonian Institution (USNM), for providing Hoba, Iquique, Santa Clara, Tawallah Valley and Tlacotepec; Denton Ebel and Joe Boesenberg, American Museum of Natural History (AMNH), New York, for Warburton Range and Skookum; F. Brandstatter, Naturhistorisches Museum Wien, Austria, for Cape of Good Hope; Rhiannon Mayne, Oscar G. Monnig Collection at Texas Christian University, for Tinnie; Lora V. Bleacher, Center for Meteorite Studies, Arizona State University, for Weaver Mountains; Carl Francis, Harvard Mineralogical Museum, for Kokomo. We thank Jozef Masarik for providing the particle spectra used in the nuclear spallation model. We thank James M.D. Day, Tim Elliott and an anonymous reviewer for their constructive reviews of the manuscript. A special thanks to Editor Tim Elliott for his efficient handling of the Pt isotope manuscripts of Kruijer et al. (this volume) and this contribution.

Appendix A. Supporting information

Supplementary data associated with this article can be found in the online version at http://dx.doi.org/10.1016/j.epsl.2012.10.013.

References

Ammon, K., Masarik, J., Leya, I., 2009. New model calculations for the production rates of cosmogenic nuclides in iron meteorites. Meteorit. Planet. Sci. 44, 485–503.
Arlandini, C., Käppeler, F., Wisshak, K., Gallino, R., Lugaro, M., Busso, M., Straniero, O., 1999. Neutron capture in low-mass asymptotic giant branch stars: cross sections and abundance signatures. Astrophys J. 525, 886–900.
Bao, Z.Y., Beer, H., Käppeler, F., Voss, F., Wisshak, K., 2000. Neutron cross sections for nucleosynthesis studies. At. Data Nucl. Data Tables 76, 70–154.
Blichert-Toft, J., Moynier, F., Lee, C.-T.A., Telouk, P., Albarède, F., 2010. The early formation of the IVA iron meteorite parent body. Earth Planet. Sci. Lett. 296, 469–480.
Burkhardt, C., Kleine, T., Bourdon, B., Palme, H., Zipfel, J., Friedrich, J.M., Ebel, D.S., 2008. Hf–W mineral isochron for Ca, Al-rich inclusions: age of the solar system and the timing of core formation in planetesimals. Geochim. Cosmochim. Acta 72, 6177–6197.
Burkhardt, C., Kleine, T., Oberli, F., Pack, A., Bourdon, B., Wieler, R., 2011. Molybdenum isotope anomalies in meteorites: constraints on solar nebula evolution and origin of the Earth. Earth Planet. Sci. Lett. 312, 390–400.
Burkhardt, C., Kleine, T., Dauphas, N., Wieler, R., 2012. Nucleosynthetic tungsten isotope anomalies in acid leachates of the Murchison chondrite: implications for hafnium-tungsten chronometry. Astrophys. J. Lett. 753 (L6) 6p.
Brandon, A., Humayun, M., Puchtel, I.S., Leya, I., Zolensky, M., 2005. Osmium isotope evidence for an s-process carrier in primitive chondrites. Science 309, 1233–1236.
Campbell, A.J., Humayun, M., 2005. Compositions of group IVB iron meteorites and their parent melt. Geochim. Cosmochim. Acta 69, 4733–4744.
Chen, J.H., Papanastassiou, D.A., Wasserburg, G.J., 2010. Ruthenium endemic isotope effects in chondrites and differentiated meteorites. Geochim. Cosmochim. Acta 74, 3851–3862.
Cohen, A.S., Waters, F.G., 1996. Separation of osmium from geological materials by solvent extraction for analysis by thermal ionisation mass spectrometry. Anal. Chim. Acta 332, 269–275.
Dauphas, N., Marty, B., Reisberg, L., 2002a. Inference on terrestrial genesis from molybdenum isotope systematics. Geophys. Res. Lett., 29.
Dauphas, N., Marty, M., Reisberg, L., 2002b. Molybdenum nucleosynthetic dichotomy revealed in primitive meteorites. Astrophys J. 569, L139–L142.
Eugster, O., 2003. Cosmic-ray exposure ages of meteorites and lunar rocks and their significance. Chem. Erde 63, 3–30.
Fischer-Gödde, Burkhardt, C., Kleine, T., 2012. Ruthenium isotope anomalies in meteorites and the cosmic Mo–Ru correlation. Lunar Planet. Sci. XLIII. (Abstract # 2492).
Harper Jr, C.L., Jacobsen, S.B., 1996. Evidence for ^{182}Hf in the early Solar System and constraints on the timescale of terrestrial accretion and core formation. Geochim. Cosmochim. Acta 60, 1131–1153.

Herzog, G.F., 2007. Cosmic-ray exposure ages of meteorites. In: Holland, H.D., Turekian, K.K. (Eds.), Treatise on Geochemistry. Elsevier, Amsterdam, pp. 1–36.
Horan, M.F., Smoliar, M.I., Walker, R., 1998. ^{182}W and ^{187}Re–^{187}Os systematics of iron meteorites: chronology for melting, differentiation, and crystallization in asteroids. Geochim. Cosmochim. Acta 62, 545–554.
Huang, S., Humayun, M., 2008. Osmium isotope anomalies in group IVB irons: cosmogenic or nucleosynthetic contributions. Lunar Planet. Sci. XXXIX. (Abstract #1168).
Humayun, M., Brandon, A.D., 2007. s-process implications from Os isotope anomalies in chondrites. Astrophys J. Lett. 664, L59–L62.
Humayun, M., Simon, S.B., Grossman, L., 2007. Tungsten and hafnium distribution in calcium–aluminum inclusions (CAIs) from Allende and Efremovka. Geochim. Cosmochim. Acta 71, 4609–4627.
Irisawa, K., Yin, Q.-Z., Hirata, T., 2009. Discovery of non-radiogenic tungsten isotopic anomalies in the Allende CV3 chondrite. Geochem. J. 43, 395–402.
Jacobsen, S.B., 2005. The Hf–W isotope system and the origin of the Earth and Moon. Annu. Rev. Earth Planet. Sci. 33, 531–570.
Kleine, T., Mezger, K., Münker, C., Palme, H., Bischoff, A., 2004. ^{182}Hf–^{182}W isotope systematics of chondrites, eucrites, and martian meteorites: chronology of core formation and early mantle differentiation in Vesta and Mars. Geochim. Cosmochim. Acta 68, 2935–2946.
Kleine, T., Mezger, K., Palme, H., Scherer, E., Münker, C., 2005. Early core formation in asteroids and late accretion of chondrite parent bodies: evidence from ^{182}Hf–^{182}W in CAIs, metal-rich chondrites, and iron meteorites. Geochim. Cosmochim. Acta 69, 5805–5815.
Kleine, T., Touboul, M., Bourdon, B., Nimmo, F., Mezger, K., Palme, H., Jacobsen, S.B., Yin, Q.-Z., Halliday, A.N., 2009. Hf–W chronology of the accretion and early evolution of asteroids and terrestrial planets. Geochim. Cosmochim. Acta 73, 5150–5188.
Kruijer, T., Sprung, P., Kleine, T., Leya, I., Wieler, R., 2011. Hf-W evidence for rapid accretion and core formation in protoplanets, Mineralogical Magazine Prague, p. 1245.
Lavielle, B., Marti, K., Jeannot, J.-P., Nishiizumi, M., Caffee, M., 1999. The 36Cl–36Ar–40K–41K records and cosmic ray production rates in iron meteorites. Earth Planet. Sci. Lett. 170, 93–104.
Lee, D.-C., Halliday, A.N., 1996. Hf–W isotopic evidence for rapid accretion and differentiation in the early solar system. Science 274, 1876–1879.
Leya, I., Wieler, R., Halliday, A.N., 2003. The influence of cosmic-ray production on extinct nuclide systems. Geochim. Cosmochim. Acta 67, 529–541.
Markowski, A., Leya, I., Quitte, G., Ammon, K., Halliday, A.N., Wieler, R., 2006a. Correlated helium-3 and tungsten isotopes in iron meteorites: quantitative cosmogenic corrections and planetesimal formation times. Earth Planet. Sci. Lett. 250, 104–115.
Markowski, A., Quitte, G., Halliday, A.N., Kleine, T., 2006b. Tungsten isotopic compositions of iron meteorites: chronological constraints vs. cosmogenic effects. Earth Planet. Sci. Lett. 242, 1–15.
Masarik, J., 1997. Contribution of neutron-capture reactions to observed tungsten isotopic ratios. Earth Planet. Sci. Lett. 152, 181–185.
Mughabghab, S.F., 2003. The thermal neutron capture cross sections resonance integrals and G-factors. International Atomic Energy Agency (Internatonal Nuclear Data Commitee), pp. 1–31.
Puchtel, I.S., Humayun, M., 2001. Platinum group element fractionation in a komatiitic basalt lava lake. Geochim. Cosmochim. Acta 65, 2979–2993.
Qin, L., Dauphas, N., Wadhwa, M., Markowski, A., Gallino, R., 2008a. Tungsten nuclear anomalies in planetesimal cores. Astrophys J. 674, 1234–1241.
Qin, L., Dauphas., N., Wadhwa, Masarik, J., Janney, P.E., 2008b. Rapid accretion and differentiation of iron meteorite parent bodies inferred from ^{182}Hf–^{182}W chronometry and thermal modeling. Earth Planet. Sci. Lett. 273, 94–104.
Reisberg, L., Dauphas, N., Luguet, A., Pearson, D.G., Gallino, R., Zimmermann, C., 2009. Nucleosynthetic osmium isotope anomalies in acid leachates of the Murchison meteorite. Earth Planet. Sci. Lett. 277, 334–344.
Rosman, K.J.R., Taylor, P.D.P., 1997. Isotopic composition of the elements 1997. Subcommittee for Isotopic Abundance Measurements, pp. 1–22.
Scherstén, A., Elliott, T., Hawkesworth, C., Russell, S., Masarik, J., 2006. Hf–W evidence for rapid differentiation of iron meteorite parent bodies. Earth Planet. Sci. Lett. 241, 530–542.
Schulz, T., Upadhyayb, D., Muenker, C., Mezger, K., 2012. Formation and exposure history of non-magmatic iron meteorites and winonaites: clues from Sm and W isotopes. Geochim. Cosmochim. Acta 85, 200–212.
Shirai, N., Humayun, M., 2011. Mass independent bias in W isotopes in MC-ICP-MS instruments. J. Anal. Atom. Spectrom. 26, 1414–1420.
Shirey, S.B., Walker, R.J., 1995. Carius tube digestions for low-blank Rhenium-Osmium analysis. Anal. Chem. 67, 2136–2141.
van Acken, D., Brandon, A.D., Humayun, M., 2011. High-precision osmium isotopes in enstatite and rumuruti chondrites. Geochim. Cosmochim. Acta 75, 4020–4036.
Volkening, J., Walczyk, T., Heumann, K.G., 1991. Osmium isotope ratio determinations by negative thermal ionization mass spectrometry. Int. J. Mass Spectrom. Ion Process. 105, 147–159.
Voshage, H., 1984. Investigations of cosmic-ray-produced nuclides in iron meteorites, 6. The Signer–Nier model and the history of the cosmic radiation. Earth Planet. Sci. Lett. 71, 181–194.
Voshage, H., Feldmann, H., 1979. Investigations on cosmic-ray-produced nuclides in iron meteorites, 3. Exposure ages, meteoroid sizes and sample depths determined by mass spectrometric analyses of potassium and rare gases. Earth Planet. Sci. Lett. 45, 293–308.
Walker, R.J., McDonough, W.F., Honesto, J., Chabot, N.L., McCoy, T.J., Ash, R.D., Bellucci, J.J., 2008. Modeling fractional crystallization of group IVB iron meteorites. Geochim. Cosmochim. Acta 72, 2198–2216.
Walker, R.J., 2012. Evidence for homogeneous distribution of osmium in the protosolar nebular. Earth Planet. Sci. Lett. 315–352, 36–44.
Yin, Q.Z., Jacobsen, S.B., Yamashita, K., Blichert-Toft, J., Telouk, P., Albarède, F., 2002. A short time-scale for terrestrial planet formation from Hf–W chronometry of meteorites. Nature 418, 949–952.
Yokoyama, T., Rai, V.K., Alexander, C.M.O.'.D., Lewis, R.S., Carlson, R.W., Shirey, S.B., Thiemens, M.H., Walker, R.J., 2007. Osmium isotope evidence for uniform distribution of s- and r-process components in the early solar system. Earth Planet. Sci. Lett. 259, 567–580.
Yokoyama, T., Alexander, C.M.O'.D., Walker, R.J., 2010. Osmium isotope anomalies in chondrites: results for acid residues and related leachates. Earth Planet. Sci. Lett. 291, 48–59.